Scuola di Dottorato in Fisica Applicata “G. Galilei” - a.a. 2004/05

Topics in Nanotechnology – part 4

Version 1, May 2005

Francesco Fuso, tel 0502214305, 0502214293 - fuso@df.unipi.it
http://www.df.unipi.it/~fuso/dida

Quantum confinement and electron transport in nanostructures

9/5/2005 – 16-18 – room T1

Outlook

• Dimensionality of the structures and density of states for 3-D, 2-D, 1-D, 0-D structures (bulk, quantum wells, quantum wires, quantum dots)

• Electron transport and quantum confinement in 2-D structures in the presence of a magnetic field:

- High mobility 2-D electron gases at heterostructure interface;
- Quantum electron in a magnetic field: Landau levels;
- Quantum Hall Effect (integer, and a few words on the fractional effect);
- von Klitzing quantum of resistance

• Electron transport and quantum confinement in 1-D structures without magnetic field:

- A few hints on practical realizations;
- Landauer treatment and levels;
- electron waveguides: “transverse modes”

• Alternative realizations of 1-D structures: a few words on carbon nanotubes and their exploitation

Conductivity in the classical (macroscopic) world

(Microscopic) Ohm's law:
J = σ **E** → I = V/R with R = l/S σ

In classical terms, resistance is a function of the dimensions (in bulk 3D materials, it is directly proportional to the length l and inversely proportional to the cross section S): **R ~ (typical width)^(2-dimensionality)**

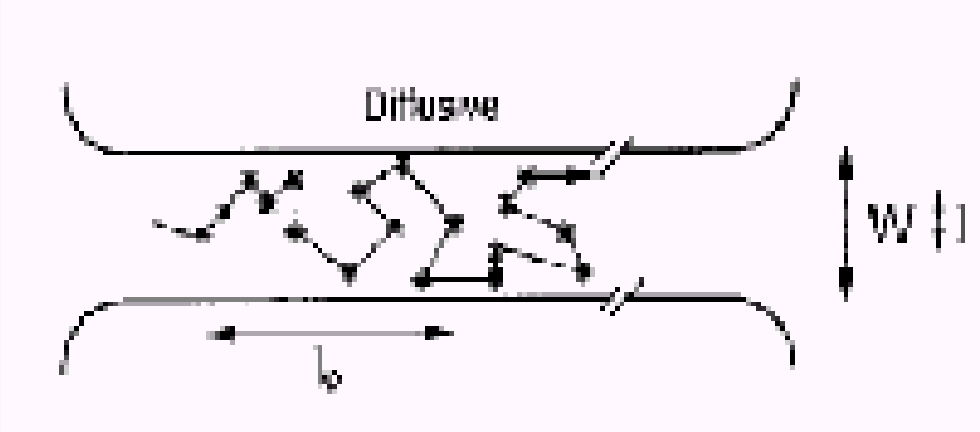

Drude (either classical or quantum):
Diffusional motion of the electrons

"Collisiona" processes (material-dependent) rule the resistivity

Dimensionality enters transport properties

Dimensionality and quantum confinement effects

Quantum confinement effects expected whenever the de Broglie wavelength of the particle (i.e., the electron) exceeds the typical size of the nanostructure

$\lambda_{dB} = h/p \sim 7x10^{-4}/v$ [m/s] in nm
($v_{term} \sim 10^4 - 10^5$ m/s, $v_F \sim 10^6$ m/s)

$$g(p)\,dp \propto \begin{cases} L/h\,dp & \text{1-D} \\ S/h^2\,2\pi p\,dp & \text{2-D} \\ V/h^3\,4\pi p^2\,dp & \text{3-D} \end{cases}$$

$$g(E)\,dE \propto \begin{cases} dE/\sqrt{E} & \text{1-D} \\ dE & \text{2-D} \\ \sqrt{E}\,dE & \text{3-D} \end{cases}$$

DOS expression affected by dimensions

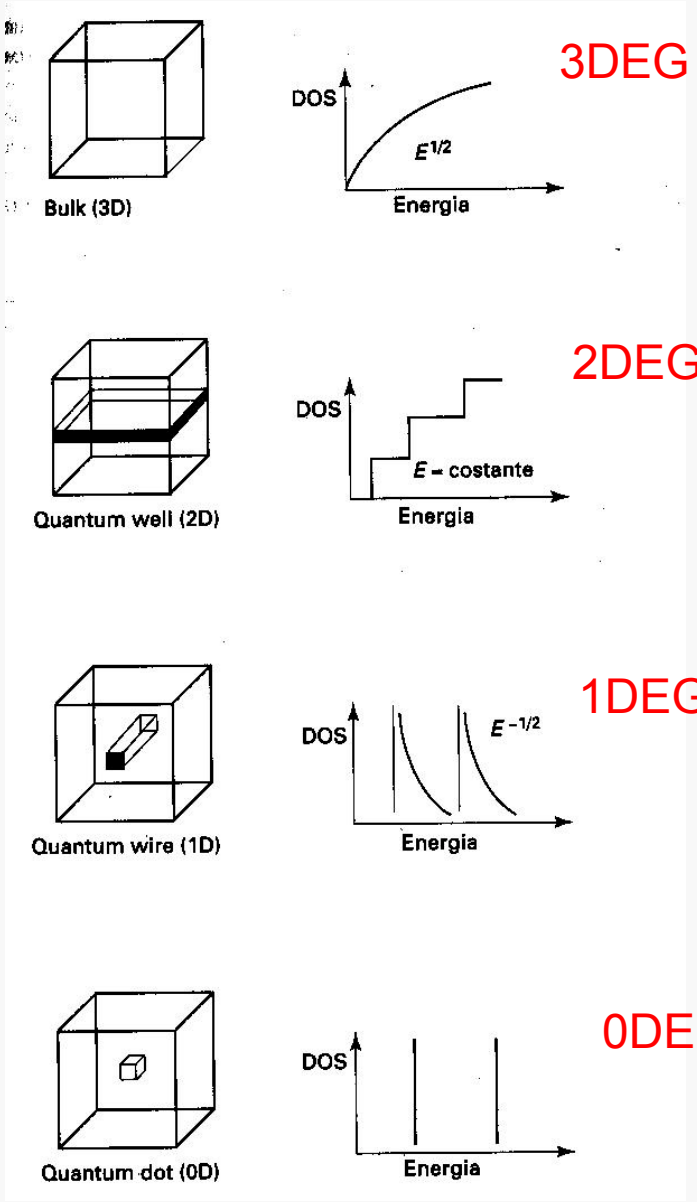

Electron transport and quantum confinement

Transport properties depend on the dimensionality of the structures: new and unexpected effects associated with quantum confinement can arise (similar to what is observed in optical quantum confinement devices*, but size must be smaller for effects to take place in electron transport*, since de Broglie wavelength is much smaller than (visible) e.m. radiation wavelength)

Quantum confinement is hard to be seen in 2DEG (2-dimension electron gases, e.g., conductive films)

Fully localized 0DEG structures (quantum dots) do require other processes for transport tooccurr (e.g., tunneling, as we will see in the next part)

Basically, 1DEG structures are well suited for investigating electron transport (quantum wires)

Hystorically, the first observations are associated with the Quantum Hall Effect (QHE) in specific 2DEG structures with the presence of a static magnetic field

2DEG in semiconducting heterostructures

1.1 Two-dimensional electron gas (2-DEG)

Recent work on mesoscopic conductors has largely been based on GaAs–AlGaAs heterojunctions where a thin two-dimensional conducting layer is formed at the interface between GaAs and AlGaAs. To understand why this layer is formed consider the conduction and valence band line-up in the z-direction when we first bring the layers in contact (Fig. 1.1.1a). The Fermi energy E_f in the widegap AlGaAs layer is higher than that in the narrowgap GaAs layer. Consequently electrons spill over from the n-AlGaAs leaving behind positively charged donors. This space charge gives rise to an electrostatic potential that causes the bands to bend as shown. At equilibrium the Fermi energy is constant everywhere. The electron density is sharply peaked near the GaAs–AlGaAs interface (where the Fermi energy is inside the conduction band) forming a thin conducting layer which is usually referred to as the two-dimensional electron gas (2-DEG in short). The carrier concentration in a 2-DEG typically ranges from $2 \times 10^{11}/\text{cm}^2$ to $2 \times 10^{12}/\text{cm}^2$ and can be depleted by applying a negative voltage to a metallic gate deposited on the surface. The practical importance of this structure lies in its use as a field effect transistor [1.2, 1.3] which goes under a variety of names such as MODFET (MOdulation Doped Field Effect Transistor) or HEMT (High Electron Mobility Transistor).

Note that this structure is similar to standard silicon MOSFETs, where the 2-DEG is formed in silicon instead of GaAs. The role of the wide-gap AlGaAs is played by a thermally grown oxide layer (SiO_x). Indeed much of the pioneering work on the properties of two-dimensional conductors was performed using silicon MOSFETs [1.4]

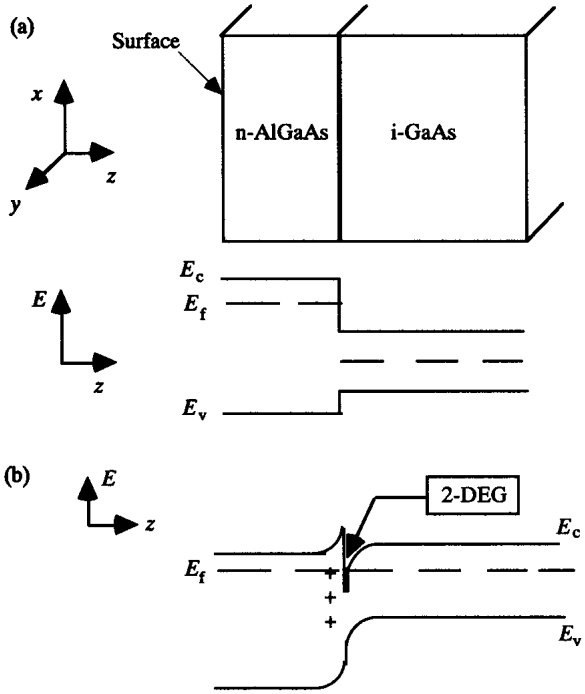

Fig. 1.1.1. Conduction and valence band line-up at a junction between an n-type AlGaAs and intrinsic GaAs, (*a*) before and (*b*) after charge transfer has taken place. Note that this is a cross-sectional view. Patterning (as shown in Fig. 0.3) is done on the surface (x–y plane) using lithographic techniques.

After S.Datta, Electronic Transport in Mesoscopic Systems, Cmbridge (1997)

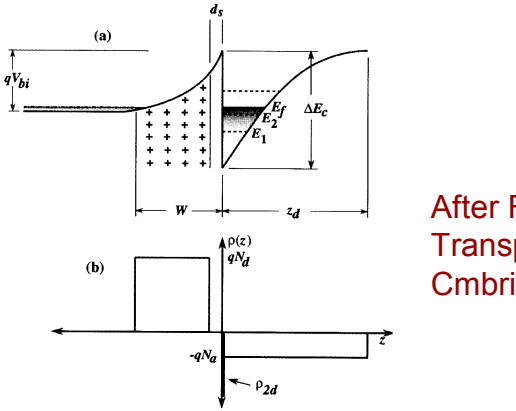

ig. 2.12. (a) Conduction band profile through a modulation-doped heterojunction system. (b) Charge ensity versus distance due to ionized donors and acceptors.

After Ferry and Goodnick, Transport in nanostructures, Cmbridge (1997)

"Band bending" at the interface produces loalization in a 2DEG with typ. thickness 1-10 nm

High mobility in MODFET/HEMT structures

Mobility

What makes the 2-DEG in GaAs very special is the extremely low scattering rates that have been achieved. The mobility (at low temperatures) provides a direct measure of the momentum relaxation time as limited by impurities and defects. Let us first briefly explain the meaning of mobility. In equilibrium the conduction electrons move around randomly not producing any current in any direction. An applied electric field **E** gives them a drift velocity $\mathbf{v}_d$ in the direction of the force $e\mathbf{E}$ as shown in Fig. 1.1.2. To relate the drift velocity to the electric field we note that, at

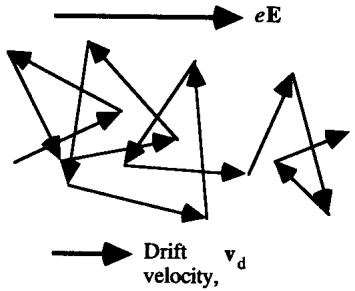

2DEG interface is much "better" than grown thin films in terms of mobility

Fig. 1.1.2. In the presence of an electric field the electrons acquire a drift velocity superposed on their random motion.

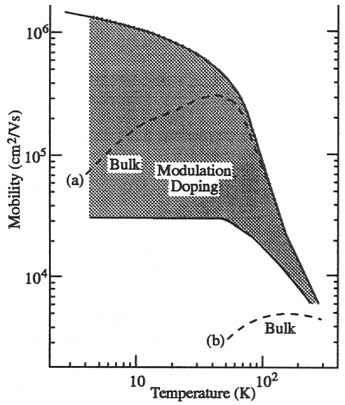

Fig. 1.1.3. Mobility vs. temperature in modulation-doped structures. Higher mobility (but lower carrier concentration) is obtained with thicker buffer layers. Also shown for comparison is the mobility in (a) high purity bulk GaAs and in (b) doped GaAs for use in FETs. Adapted with permission from Fig. 9 of T. J. Drummond, W. T. Masselink and H. Morkoc (1986). *Proc. IEEE*, **74**, 779. © 1986 IEEE

High "in-plane" mobility achieved (collisions negligible)

steady-state, the rate at which the electrons receive momentum from the external field is exactly equal to the rate at which they lose momentum (**p**) due to scattering forces:

$$\left[\frac{d\mathbf{p}}{dt}\right]_{\text{scattering}} = \left[\frac{d\mathbf{p}}{dt}\right]_{\text{field}}$$

Hence, (τ_m: momentum relaxation time)

$$\frac{m\mathbf{v}_d}{\tau_m} = e\mathbf{E} \quad \Rightarrow \quad \mathbf{v}_d = \frac{e\tau_m}{m}\mathbf{E}$$

The mobility is defined as the ratio of the drift velocity to the electric field:

$$\mu \equiv \left|\frac{v_d}{E}\right| = \frac{|e|\tau_m}{m} \qquad (1.1.1)$$

Mobility measurement using the Hall effect (see Section 1.5) is a basic characterization tool for semiconducting films. Once the mobility is known, the momentum relaxation time is readily deduced from Eq.(1.1.1).

In bulk semiconductors as we go down from room temperature, the momentum relaxation time increases at first due to the suppression of phonon scattering. But it does not increase any further once the phonon scattering is small enough that impurity scattering becomes the dominant mechanism (see Fig. 1.1.3). With a donor concentration of $10^{17}/\text{cm}^3$ the highest mobility is less than 10^4 cm^2/V s. Higher mobilities can be obtained with undoped samples but this is not very useful since there are very few conduction electrons.

In a 2-DEG, on the other hand, carrier concentrations of $10^{12}/\text{cm}^2$ in a layer of thickness ~100 Å (equivalent bulk concentration of $10^{18}/\text{cm}^3$) have been obtained with mobilities in excess of 10^6 cm^2/V s (the current record is almost an order of magnitude larger than what is shown in Fig. 1.1.3). The reason is the spatial separation between the donor atoms in the AlGaAs layer and the conduction electrons in the GaAs layer. This reduces the scattering cross-section due to the impurities, leading to weaker scattering. Often an extra buffer layer of undoped AlGaAs is introduced between the GaAs and the n-AlGaAs in order to increase the separation between the 2-DEG in the GaAs and the ionized donors in the AlGaAs. This reduces the scattering but it also reduces the carrier concentration.

Classical Hall effect in a conductor

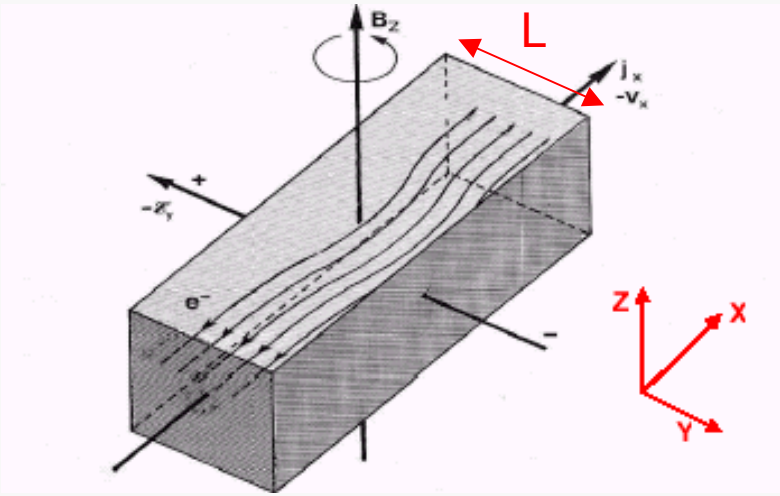

$$V_H = R_H I = v_d B L = \mu B L / e$$

Mobility can be measured (including the sign) by Hall experiments

Classically, the Hall resistance is a continuous feature depending on the mobility

A known current is sent along *x*

A known magnetic field (static and homogeneous) is applied along *z*

In a two-charge fluid model of the current, Lorentz force drives positive and negative charge along *y*, with a sign depending on the charge polarity

At equilibrium, charge separation occurs (along *y*)
-> an electric field exists
-> a potential difference can be measured across *y* direction

Electron dynamics in a magnetic field (quantum)

Effetti quantistici: diventano importanti ad esempio quando la separazione dei livelli energetici quantizzati è paragonabile a energia del sistema, oppure quando la lunghezza d'onda di de Broglie $\lambda_{dB} = h/p$ si avvicina ad una lunghezza caratteristica del sistema.

Nel QHE si ha quantizzazione dell'energia dovuta alla presenza di B, che produce effetti osservabili (anche per valori di campo *realistici*) grazie alle piccole dimensioni del sistema in una direzione.

0.1 Moto classico di un elettrone in presenza di B

Suppongo **B**= B **2**. Dalla forza di Lorentz

$$\mathbf{F}_{Lorentz} = -e\mathbf{v} \times \mathbf{B} \qquad (1)$$

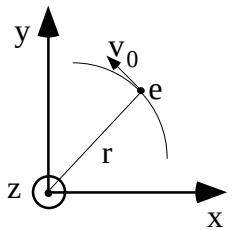

si ha:

$$m\dot{v}_x = -ev_y B \qquad (2)$$
$$m\dot{v}_y = ev_x B\,, \qquad (3)$$

da cui (derivando e sostituendo):

$$m\ddot{v}_x = -\frac{e^2B^2}{m}v_x\,. \qquad (4)$$

Il moto lungo x ed y è oscillatorio con la pulsazione di ciclotrone $\omega_c = eB/m$. La combinazione dei moti lungo x ed y con opportune condizioni iniziali dà luogo ad uno moto circolare con la stessa pulsazione e *raggio arbitrario* (purché $\omega_c = v_0/r$). Se l'elettrone ha anche moto lungo z, la traiettoria è una spirale.

0.2 Trattazione quantistica

L'Hamiltoniana di un elettrone in presenza di B è (gauge di Lorentz):

$$\mathcal{H} = \frac{1}{2m}(\mathbf{p} - e\mathbf{A})^2\,, \qquad (5)$$

con **A** potenziale vettore ($\nabla \times \mathbf{A} = \mathbf{B}$). Nel nostro caso conviene scegliere $\mathbf{A} = (-By, 0, 0)$, quindi si ha:

$$\mathcal{H} = \frac{1}{2m}((p_x + eBy)^2 + p_y^2 + p_z^2)\,. \qquad (6)$$

Dato che non compare dipendenza esplicita né da x né da z, p_x e p_z sono costanti del moto, quindi la soluzione sarà del tipo $\psi = \exp(ik_x x)\exp(ik_z z)\mathcal{F}(y)$, con $\mathcal{F}(y)$ funzione da determinare attraverso l'applicazione dell'eq. di Schrödinger (Eq. 6), che dà:

$$-\frac{\hbar^2}{2m}\frac{\partial^2\mathcal{F}}{\partial y^2} + \frac{1}{2}m\omega_c^2(y - y_0)^2\mathcal{F} = E'\mathcal{F}\,, \qquad (7)$$

con E' espressione opportuna di energia. Questa è l'equazione di un oscillatore armonico lungo y con pulsazione ω_c e *centro di oscillazione*:

$$y_0 = -\frac{\hbar k_x}{eB}\,. \qquad (8)$$

I livelli di energia sono quantizzati con autovalori:

$$E_{n,j} = E_{kin} + (n + \frac{1}{2})\hbar\omega_c\,, \qquad (9)$$

dove j è un numero quantico riferito all'energia cinetica E_{kin}. Si noti che i valori del quanto di energia sono genralmente bassi (meV o frazioni di meV) per campi magnetici usuali.

Se il sistema ha piccole dimensioni lungo y (supponiamo lo spessore sia L), allora deve essere $|y_0| \leq L$, da cui:

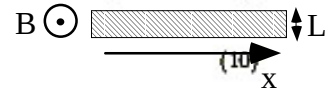

$$k_x < \frac{eBL}{\hbar} = \frac{\omega_c m L}{\hbar}\,. \qquad (10)$$

Quindi, la bassa dimensionalità lungo y produce una limitazione sul valore di k_x (effetto di "mescolamento" delle direzioni spaziali tipico delle situazioni in cui si ha a che fare con un campo magnetico).

0.3 Densità degli stati e degenerazione

Nel caso unidmensionale, che qui si applica per tenere conto del confinamento spaziale lungo la direzione y, e di conseguenza del confinamento nello spazio k lungo la direzione x (vedi Eq. (10)), si ha che la densità degli stati (riferita solo alla direzione di quantizzazione) è:

$$g(k_x)dk_x = dk_x\frac{L}{2\pi}\,. \qquad (11)$$

Considerando la sola direzione x, integrando si ottiene:

$$\int_0^{k} dk_x\frac{L}{2\pi} = \frac{eBL^2}{2\pi\hbar}\,, \qquad (12)$$

dove si è tenuto conto della condizione Eq. (10). Dividendo l'espressione al membro di destra di Eq. (12) per L^2 si ottiene in pratica una densità (n_s) di portatori di carica per unità di superficie (reale), che vale quindi:

$$n_s = \frac{eB}{2\pi\hbar}\,. \qquad (13)$$

Landau levels

D'altra parte, l'energia del portatore di carica si può scrivere

$$E = E_n + \frac{\hbar^2 k_x^2}{2m}, \qquad (14)$$

dove rispetto alla Eq. (14) si è esplicitata la parte cinetica. Dalla Eq. (14) si ricava

$$dk_x = \frac{\sqrt{2m}}{2\hbar}\frac{1}{\sqrt{E - E_n}}dE \qquad (15)$$

da cui

$$g(E) \propto \frac{1}{\sqrt{E - E_n}}, \qquad (16)$$

densità degli stati tipica per un gase 1-DEG. In corrispondenza delle energie E_n la $g(E)$ tende a divergere (livelli di Landau).

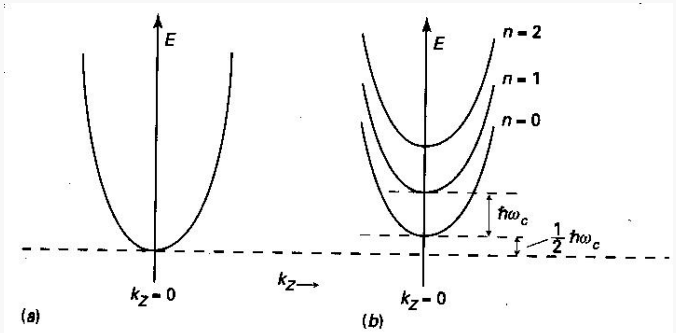

Figura 9.3
Schema di bande di energia in funzione di k_z in assenza (*a*) ed in presenza (*b*) di un campo magnetico $\overline{B}$ applicato in direzione z (vedi eq. 9.52).

1D-like density of states

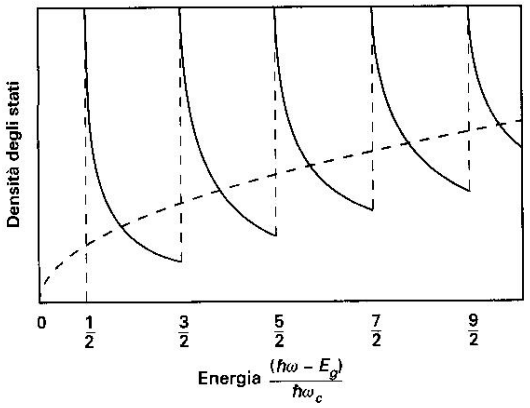

Figura 9.5
Densità di stati vicino al minimo di una banda in presenza di un campo magnetico costante: il caso $B = 0$ è indicato con linea tratteggiata (vedi eq. 8.25) e il caso $B \neq 0$ con linea continua (vedi eq. 9.58).

(Surface) density of states corresponding to Landau levels is eB/h

Number of electrons involved in conductivity, which depends on the (surface) density of states, gets a quantized behavior as a function of the energy

The small thickness of the conductor combined with the presence of the magnetic field leads to a 1D-like behavior

QHE and von Klitzing quantum of resistance I

0.4 Quanto di resistenza di Von Klitzing

Considerando la forza di Lorentz come forza elettromotrice, nell'effetto Hall classico si ha che la differenza di potenziale V_H (in direzione y, cioè trasversa rispetto al moto delle cariche e al campo magnetico) è $V_H = LBv$ e la corrente di portatori di carica è $I = n_s veL$, con n_s densità superficiale di carica già introdotta. Dalla legge di Ohm si deduce una resistenza Hall R_H:

$$R_H = \frac{V_H}{I} = \frac{B}{n_s e} . \qquad (17)$$

Nel QHE, l'azione combinata del campo magnetico e del confinamento spaziale porta alla presenza dei livelli di Landau e alla loro degenerazione. Quando un livello di Landau (supponiamo il livello m) è completamente occupato e il successivo è completamente vuoto, cioè m livelli di Landau sono pieni, ognuno con la degenerazione vista in precedenza, allora, secondo la Eq. (13), si avrà un numero di elettroni per unità di superficie pari a:

$$n = m\frac{eB}{h} , \qquad (18)$$

da cui deriva che la resistenza Hall si esprime come sottomultiplo del valore h/e^2, dipendente solo da costanti fondamentali:

$$R_H = \frac{1}{m}\frac{h}{e^2} . \qquad (19)$$

Questo risultato ha diverse conseguenze. In primo luogo stabilisce un valore quantizzato della resistenza (il cui valore è 25812.806 ohm). Occorre notare che nell'effetto Hall quantistico la quantizzazione della resistenza é conseguenza del confinamento spaziale, ma la sua osservazione è resa possibile dalla presenza del campo magnetico (e conseguente quantizzazione del moto dei portatori di carica). In condizioni ordinarie l'effetto di quantizzazione non è facilmente osservabile (e, in generale, si ricordi che la resistenza misurata può essere interpretata come un parallelo di tante resistenze). Inoltre esistono delle conseguenze notevoli dal punto di vista metrologico, legate alla precisione con cui si può eseguire la misura delle costanti fondamentali h e e^2. Dal punto di vista tecnologico, la conseguenza principale è comunque che la differenza di potenziale misurata non è lineare con la corrente, ma segue un tipico andamento a gradini. Per ragioni di tipo sperimentale, i sistemi in cui tradizionalmente si osserva QHE sono delle eterostrutture, ad esempio tipo GaAs/GaAsAl, in cui il confinamento spaziale è ottenuto in strati sottili (pozzi quantici).

Per completezza, occorre ricordare che accanto al QHE *intero*, scoperto da Von Klitzing (premio Nobel 1985), esiste un QHE *frazionario*, legato all'occupazione frazionaria dei livelli di Landau (Tsui and Stormer, premio Nobel 1998).

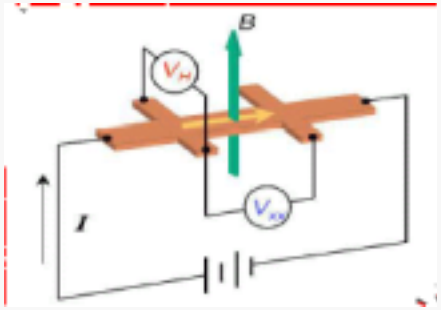

Fine structure constant

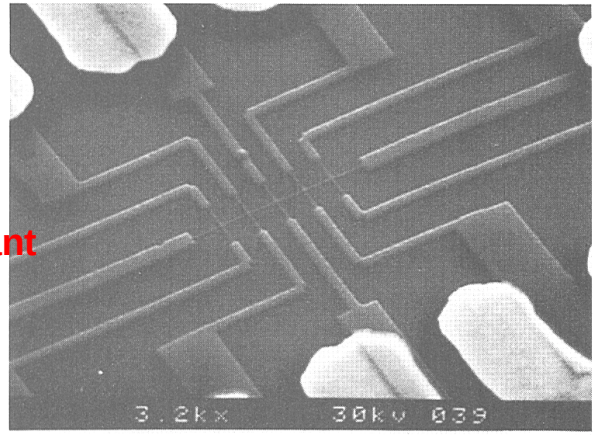

Fig. 0.3. Scanning electron micrograph of a long wire 75 nm wide patterned from a GaAs–AlGaAs heterojunction. Four-terminal Hall measurements are made using voltage probes placed along the wire ~ 2 μm. apart. Reproduced with permission from M. L. Roukes, A. Scherer, S. J. Allen, H. G. Craighead, R. M. Ruthen, E. D. Beebe and J. P. Harbison (1987), *Phys. Rev. Lett.* **59**, 3011.

Measurements carried out at very low temperature in order to decrease (phonon) scattering

QHE and von Klitzing quantum of resistance II

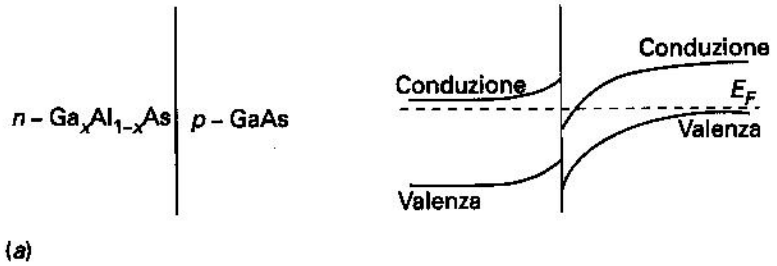

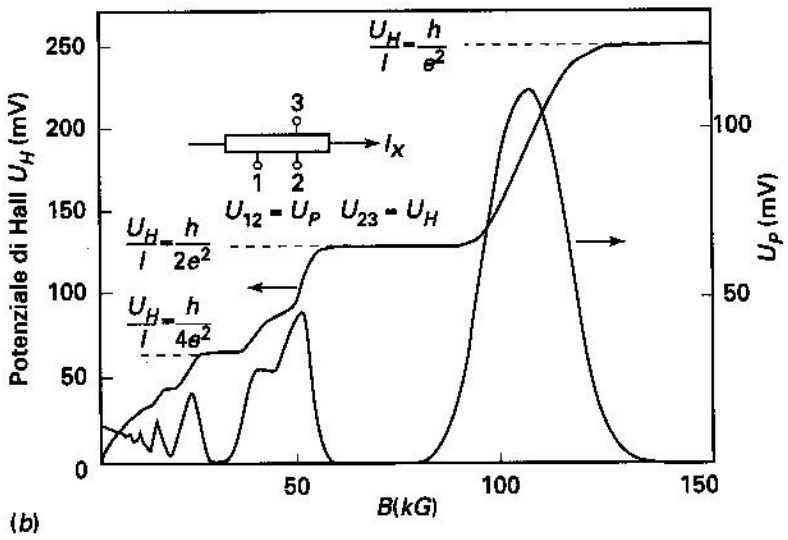

Figura 11.11
(*a*) Indicazione schematica della giunzione con campo elettrico, che produce stati con mobilità alla superficie della giunzione. (*b*) Misure di effetto Hall quantizzato, con i caratteristici gradini dove il potenziale di Hall è costante, e il potenziale nella direzione della corrente è nullo. (Da K. von Klitzing, Europhysics News **13**, 2 (Aprile 1982)).

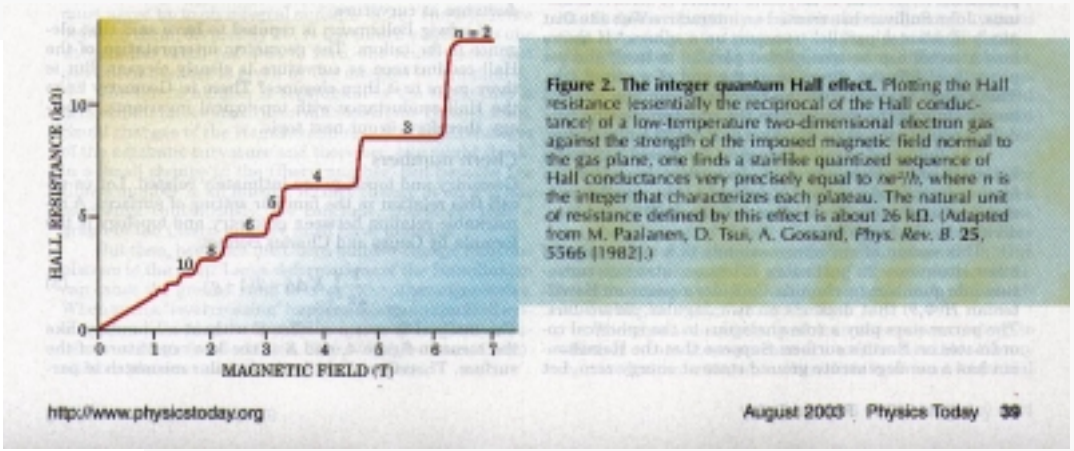

Resistance is quantized in units of R_{vk} ~ 25.8 Kohm

The quantum depends on the fine structure costant, i.e., on fundamental quantities (e, h)

A few words on fractional-QHE

1982 (Tsui, Stoermer, et al.): discovery of Fractional-QHE

$$R_H = \frac{p}{q}\frac{h}{e^2}$$

$$\nu = \frac{p}{2mp \pm 1}$$

Filling factor

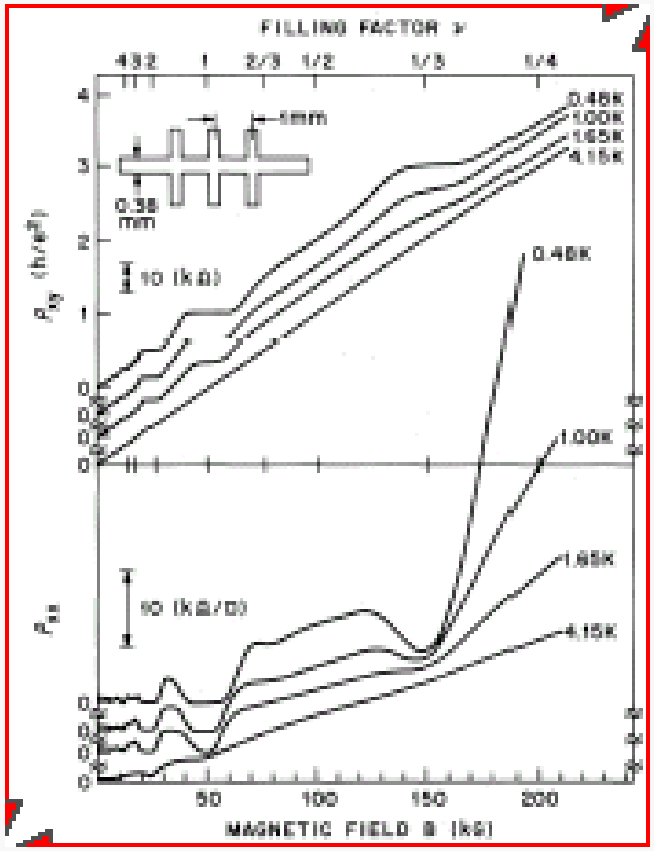

Tsui et al., PRL 48, 1559 (1982)

Interpretation (Laughlin): many-body problem

The Hamiltonian should include terms accounting for interaction inter-electron and electron-ion (lattice)

A collective wavefunction (product of single electron wavefunction) should be used and the corresponding Landau levels identified

Degeneracy of the levels turns out to depend on the specific system considered

Examples of realization of 1-D nanostructures

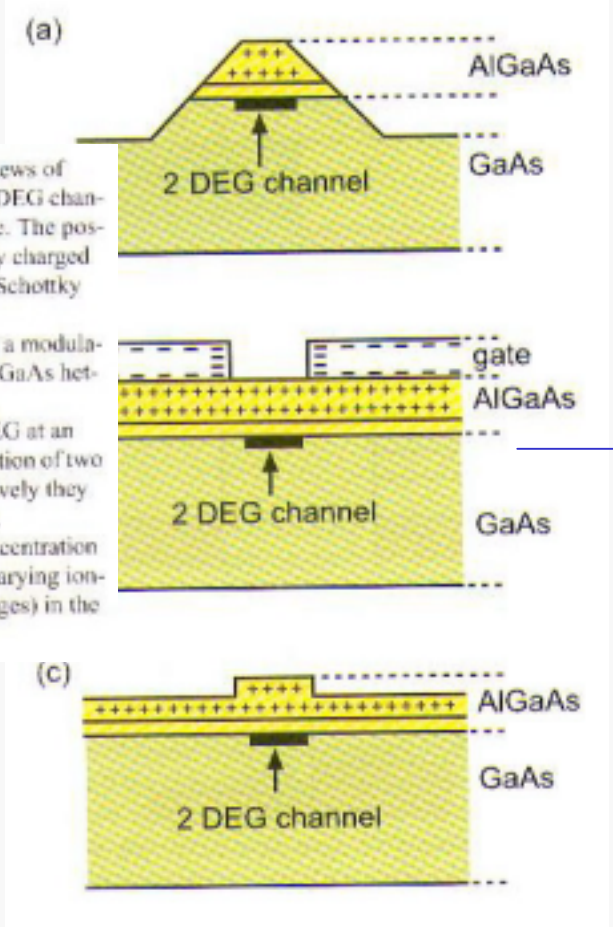

Figure 16: Schematic cross sectional views of three different ways to define narrow 2-DEG channels in an AlGaAs/GaAs heterostructure. The positively ionized donors and the negatively charged 2-DEG channel as well as the negative Schottky gate electrode (b) are indicated.
(a) Lithographically structured wire on a modulation doped (AlGaAs n-doped) AlGaAs/GaAs heterostructure.
(b) 2-DEG channel formed in the 2-DEG at an AlGaAs/GaAs heterostructure by the action of two evaporated metal gates. If biased negatively they repel the electrons in the 2-DEG below.
(c) A similar effect on the electron concentration in the 2-DEG is obtained by spatially varying ionized donor concentration (positive charges) in the upper AlGaAs layer.

Split-gate MODFET

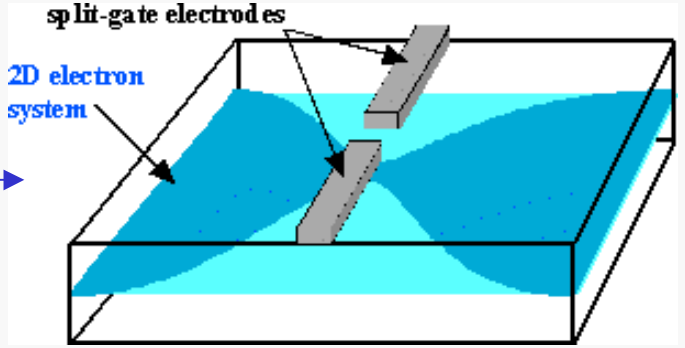

An additional pair of electrodes with a nanosized gap leads to a 1-D like conducting channel

Da R. Waser Ed., Nanoelectronics and information technology (Wiley-VCH, 2003)

A closer look to the de Broglie wavelength

Degenerate and non-degenerate conductors

At equilibrium the available states in a conductor are filled up according to the Fermi function

$$f_0(E) = \frac{1}{1+\exp\left[(E-E_f)/k_BT\right]} \qquad (1.2.7)$$

where E_f is the Fermi energy. Away from equilibrium the system has no common Fermi energy, but often we can talk in terms of a local quasi-Fermi level which can vary spatially and which can be different for different groups of states (such as electrons and holes) even at the same spatial location. We will generally use F_n to denote quasi-Fermi levels and reserve E_f for the equilibrium Fermi energy.

There are two limits in which the Fermi function inside the band ($E > E_s$) can be simplified somewhat making it easier to perform numerical calculations (see Fig. 1.2.2). One is the high temperature or the non-degenerate limit ($\exp[E_s - E_f]/k_BT >> 1$) where

$$f_0(E) \approx \exp\left[-(E-E_f)/k_BT\right] \qquad (1.2.8)$$

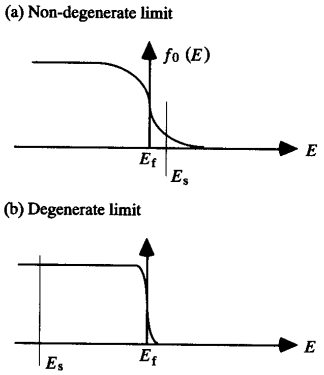

Fig. 1.2.2. The Fermi function inside the band ($E > E_s$) can be approximated by (*a*) Eq.(1.2.8) in the non-degenerate limit and (*b*) by Eq.(1.2.9) in the degenerate limit.

The other is the low temperature or the degenerate limit ($\exp[E_s - E_f]/k_BT << 1$) where

$$f_0(E) \approx \vartheta(E_f - E) \qquad (1.2.9)$$

In this book we will mainly be discussing degenerate conductors.

To relate the equilibrium electron density n_s (per unit area) to the Fermi energy we make use of the relation

$$n_s = \int N(E) f_0(E) dE$$

For degenerate conductors it is easy to perform the integral to obtain

$$n_s = N_s(E_f - E_s) \quad \text{where} \quad N_s = m/\pi\hbar^2 \qquad (1.2.10)$$

where we have made use of Eqs.(1.2.6) and (1.2.9).

At low temperatures the conductance is determined entirely by electrons with energy close to the Fermi energy. The wavenumber of such electrons is referred to as the Fermi wavenumber (k_f):

$$E_f - E_s = \frac{\hbar^2 k_f^2}{2m} \quad \Rightarrow \quad \hbar k_f = \sqrt{2m(E_f - E_s)} \qquad (1.2.11)$$

Using Eq.(1.2.10) we can express the Fermi wavenumber in terms of the electron density:

$$k_f = \sqrt{2\pi n_s} \qquad (1.2.12)$$

The corresponding velocity is the Fermi velocity $v_f = \hbar k_f / m$.

In the "degenerate case" (low temperature) Fermi velocity depends on the electron density

Criteria for 1DEG situations

1.3 Characteristic lengths

A conductor usually shows ohmic behavior if its dimensions are much larger than certain characteristic lengths, namely, (1) the de Broglie wavelength, (2) the mean free path, and (3) the phase-relaxation length. We will discuss these one by one. In addition to these characteristic lengths, the screening length can also play a significant role especially in low-dimensional conductors as we will see in Section 2.3 (see Fig. 2.3.3).

Wavelength (λ)

We have seen (Eq.(1.2.12)) that the Fermi wavenumber k_f goes up as the square root of the electron density. The corresponding wavelength goes down as the square root of the electron density:

$$\lambda_f = 2\pi/k_f = \sqrt{2\pi/n_s} \qquad (1.3.1)$$

De Broglie wavelength at the Fermi velocity

For an electron density of $5 \times 10^{11}/\text{cm}^2$, the Fermi wavelength is about 35 nm. At low temperatures the current is carried mainly by electrons having an energy close to the Fermi energy so that the Fermi wavelength is the relevant length. Other electrons with less kinetic energy have longer wavelengths but they do not contribute to the conductance.

Mean free path (L_m)

An electron in a perfect crystal moves as if it were in vacuum but with a different mass. Any deviation from perfect crystallinity such as impurities, lattice vibrations (phonons) or other electrons leads to 'collisions' that scatter the electron from one state to another thereby changing its momentum. The momentum relaxation time τ_m is related to the collision time τ_c by a relation of the form

$$\frac{1}{\tau_m} \rightarrow \frac{1}{\tau_c}\alpha_m$$

where the factor α_m (lying between 0 and 1) denotes the 'effectiveness' of an individual collision in destroying momentum. For example if the collisions are such that the electrons are scattered only by a small angle then very little momentum is lost in an individual collision. The factor α_m is then very small so that the momentum relaxation time is much longer than the collision time. For a more detailed discussion of scattering times in semiconductors see, for example, Chapter 4 of S. Datta (1989), *Quantum Phenomena*, Modular Series on Solid-state Devices, vol. VIII, eds. R. F. Pierret and G. W. Neudeck, (New York, Addison–Wesley).

The mean free path, L_m, is the distance that an electron travels before its initial momentum is destroyed; that is,

$$L_m = v_f \tau_m \qquad (1.3.2)$$

where τ_m is the momentum relaxation time and v_f is the Fermi velocity. The Fermi velocity is given by

$$v_f = \frac{\hbar k_f}{m} = \frac{\hbar}{m}\sqrt{2\pi n_s} \rightarrow 3\times10^7\,\text{cm/s} \quad \text{if} \quad n_s = 5\times10^{11}/\text{cm}^2$$

Assuming a momentum relaxation time of 100 ps we obtain a mean free path of $L_m = 30$ μm.

Phase-relaxation length (L_φ)

Let us first discuss what is meant by the phase-relaxation time (τ_φ). We will then relate it to the phase-relaxation length. In analogy with the momentum relaxation time we could write

$$\frac{1}{\tau_\varphi} \rightarrow \frac{1}{\tau_c}\alpha_\varphi$$

where the factor α_φ denotes the effectiveness of an individual collision in destroying phase. The destruction of phase is, however, a little more subtle than the destruction of momentum. A more careful discussion is required to define what the effectiveness factor α_φ is for different types of scattering processes.

A rough picture of 1DEG conductivity

In the bulk, classically we have:
J = *n* e **v**

1. At T=0 only the portion of electrons eV/ E_F is involved in the transport process
2. Fermi velocity must be considered: $v_F = \sqrt{(2E_F/m)}$;
3. $n \propto \int g(E)dE$; in the 1-D case $\propto \sqrt{E_F}$

$I = eV/E_F \; e \; \sqrt{(2E_F/m)} \; \sqrt{(2m \; E_F)}/h =$
$= 2 \; e^2 \; V/h$

Conductivity in an ideal 1DEG structure:
$G_{1D} = i/V = 2 \; e^2/h$

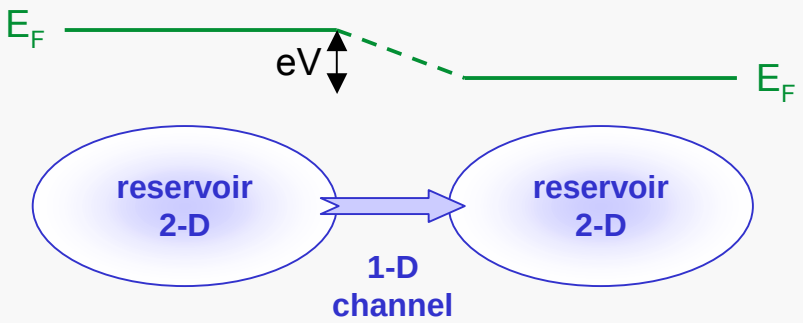

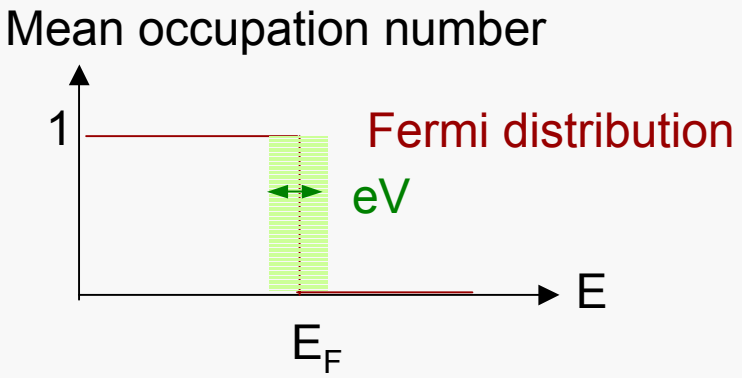

1DEG DOS peculiarities lead to a quantized conductivity

See van Wees et al.
PRL 60 848 (1988)

Landauer levels

"tunneling" through a quantum wire

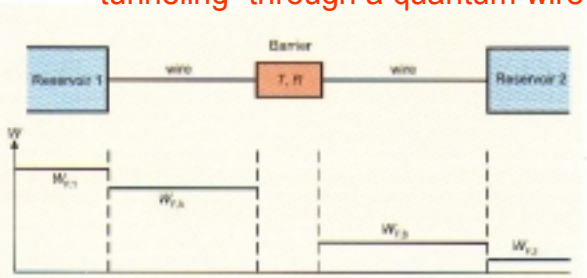

Figure 19: One-channel model for the derivation of ballistic quantum transport through a barrier between two reservoirs. The barrier is described by its transmittance T and its reflectance R. μ_1, μ_2, μ_3 and μ_4 are the chemical potentials in the different regions.

A general description of non-diffusive quantum-mechanical transport in nano- and mesoscopic structures has been developed by Landauer [9] and Büttiker [10]. In the idealized model two reservoirs 1 and 2 characterized by their chemical potentials $W_{F,1}$ and $W_{F,2}$ are connected through two ideal 1-D wires of length L. In these wires the electronic states are plane waves $\psi(x) = \exp(ikx)/\sqrt{L}$, which can have positive and negative k-vectors and two spin orientations. With the quantum-mechanical expression for the current density in one dimension

$$j = \frac{e\hbar}{2im}\left(\psi^*\nabla\psi - \psi\nabla\psi^*\right) \tag{55}$$

(quantum) current density

the corresponding current for one k-vector and one spin orientation is obtained as

$$I = \frac{e\hbar k}{mL} \tag{56}$$

Between the two wires an energetic barrier for the electrons is assumed, which is characterized by its quantum-mechanical reflection coefficient R and its transmission coefficient T, with $T + R = 1$ (Figure 19).

Due to the difference $W_{F,1} - W_{F,2}$ of the chemical potentials a current through the wires is induced. It results from electrons with energies $W_{F,1} \geq W \geq W_{F,2}$ and k-vectors in positive forward direction, which occupy the electronic states in the left wire. Part of the current is reflected at the barrier and the other part is transmitted. The reflected current is absorbed in reservoir 1 while the transmitted part is absorbed in reservoir 2. Only within these reservoirs does energy dissipation occur. The total current in the positive k-direction in the left wire is thus obtained by adding up all occupied states and using (56) as

$$I_{\rightarrow} = \frac{e\hbar k}{mL} L D^{(1)}(W)\left(W_{F,1} - W_{F,2}\right) \tag{57}$$

$D^{(1)}(W)$ is the 1-D density of states (per wire length L) according to (51). With $W = \hbar^2k^2/2m$ this yields

$$I_{\rightarrow} = \frac{e}{\pi\hbar}\left(W_{F,1} - W_{F,2}\right) \tag{58}$$

and for the transmitted net current in the right wire

$$I = \frac{e}{\pi\hbar} T\left(W_{F,1} - W_{F,2}\right) \tag{59}$$

The reflected current I_R in the left wire is accordingly

$$I_R = \frac{e}{\pi\hbar} R\left(W_{F,1} - W_{F,2}\right) \tag{60}$$

For the determination of the chemical potentials the total number of states in the wires, with positive and negative k-values, has to be taken into account, i.e. $2D^{(1)}(W)(W_{F,1} - W_{F,2})$. In the right wire the current, which is induced by $(W_{F,1} - W_{F,2})$, corresponds to a complete occupation of states between $W_{F,B}$ and $W_{F,2}$ (Figure 19), such that

$$TD^{(1)}(W)\left(W_{F,1} - W_{F,2}\right) = 2D^{(1)}(W)\left(W_{F,1} - W_{F,2}\right) \tag{61}$$

Within the left wire both the currents $I_{\rightarrow}$ and I_R have to be considered and the resulting occupation of states is assumed to correspond to the occupation of states between $W_{F,A}$ and $W_{F,2}$, such that

$$(1+R)D^{(1)}(W)\left(W_{F,1} - W_{F,2}\right) = 2D^{(1)}(W)\left(W_{F,A} - W_{F,2}\right) \tag{62}$$

With R+T = 1 the difference between (61) and (62) yields

$$W_{F,A} - W_{F,B} = R\left(W_{F,1} - W_{F,2}\right) \tag{63}$$

With V as the voltage between both wires and $eV = W_{F,A} - W_{F,B}$ one obtains from (59) and (63) for the current through the wires

$$I = \frac{e^2}{\pi\hbar}\frac{T}{R}V = \frac{2e^2}{h}\frac{T}{R}V \tag{64}$$

This is the analogue to Ohm's law for quantum transport through a nanoscopic system. The conductance of the system thus follows as

$$G = \frac{2e^2}{h}\frac{T}{R} \tag{65}$$

This so-called Landauer formula again contains the conductivity quantum e^2/h of 1-D quantum transport. The Landauer formalism for quantum transport can be generalized to a network where several wires connect a barrier with reservoirs.

Da R. Waser Ed., Nanoelectronics and information technology (Wiley-VCH, 2003)

Ballistic transport

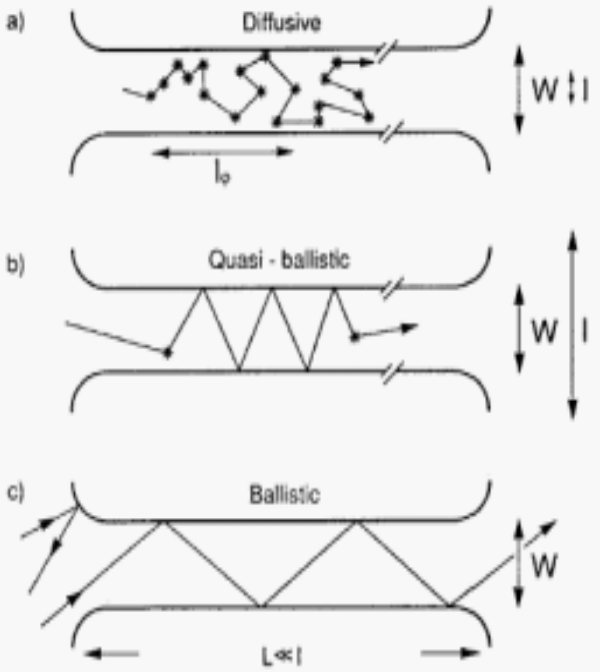

Figure 10.4: Electron trajectories characteristic of the diffusive ($\ell < W, L$), quasi-ballistic ($W < \ell < L$), and ballistic ($W, L < \ell$) transport regimes, for the case of specular boundary scattering. Boundary scattering and internal impurity scattering (asterisks) are of equal importance in the quasi-ballistic regime. A nonzero resistance in the ballistic regime results from backscattering at the connection between the narrow channel and the wide 2DEG regions. Taken from H. Van Houten et al. in "Physics and Technology of Submicron Structures" (H. Heinrich, G. Bauer and F. Kuchar, eds.) Springer, Berlin, 1988.

In the ballistic transport regime, electrons are assumed to move within the structure without scattering (but that at the interface with the ohmic contacts, i.e., the higher-dimensional "world")

Behavior analogous to an optical fiber in the total reflection mode

If a quantum wire is considered, comparison between the de Broglie wavelength and the *transverse* size suggests to consider *single mode fibers*

⇩

Transverse modes

Transverse modes I

1.6 Transverse modes (or magneto-electric subbands)

this section we will discuss the concept of transverse modes or sub-
ıds which will appear repeatedly in this book. These are analogous to transverse modes (TE_{10}, TM_{11} etc.) of electromagnetic waveguides. In row conductors, the different transverse modes are well separated in rgy and such conductors are often called *electron waveguides*.

We consider a rectangular conductor that is uniform in the x-direction and has some transverse confining potential $U(y)$ (see Fig. 1.6.1). The motion of electrons in such a conductor is described by the effective mass equation (see Eq.(1.2.2))

$$\left[E_s + \frac{(i\hbar\nabla + eA)^2}{2m} + U(y)\right]\Psi(x,y) = E\Psi(x,y)$$

We assume a constant magnetic field B in the z-direction perpendicular to the plane of the conductor. This can be represented by a vector potential of the form

$$\mathbf{A} = -\hat{x}By \quad \Rightarrow \quad A_x = -By \quad \text{and} \quad A_y = 0$$

so that Eq.(1.2.2) can be rewritten as

$$\left[E_s + \frac{(p_x + eBy)^2}{2m} + \frac{p_y^2}{2m} + U(y)\right]\Psi(x,y) = E\Psi(x,y) \qquad (1.6.1)$$

where $$p_x = -i\hbar\frac{\partial}{\partial x} \quad \text{and} \quad p_y = -i\hbar\frac{\partial}{\partial y}$$

The solutions to Eq.(1.6.1) can be expressed in the form of plane waves (L: length of conductor over which the wavefunctions are normalized)

$$\Psi(x,y) = \frac{1}{\sqrt{L}}\exp[ikx]\chi(y) \qquad (1.6.2)$$

where the transverse function $\chi(y)$ satisfies the equation

$$\left[E_s + \frac{(\hbar k + eBy)^2}{2m} + \frac{p_y^2}{2m} + U(y)\right]\chi(y) = E\chi(y) \qquad (1.6.3)$$

Note that the choice of vector potential is not unique for the given magnetic field. For example we could choose $A_x = 0$ and $A_y = -Bx$. The solutions would then look very different though the physics of course must remain the same. It is only with our choice of gauge, that the solutions have the form of plane waves in the x-direction. We will use this gauge in all our discussions.

We are interested in the nature of the transverse eigenfunctions and the eigenenergies for different combinations of the confining potential U and the magnetic field B. In general for arbitrary confinement potentials $U(y)$

ere are no analytical solutions. However, for a parabolic potential hich is often a good description of the actual potential in many elec-
ın waveguides)

$$U(y) = \frac{1}{2}m\omega_0^2 y^2$$

Confining potential

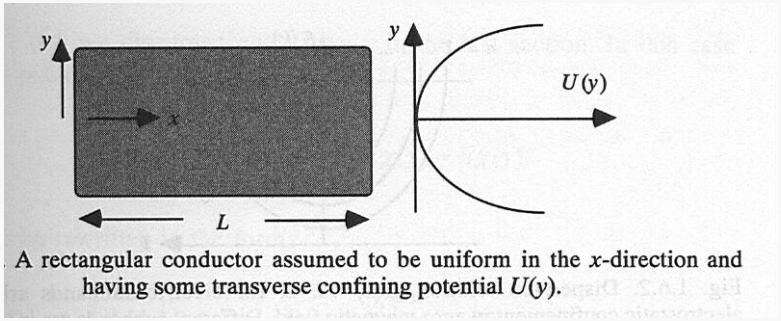

A rectangular conductor assumed to be uniform in the x-direction and having some transverse confining potential $U(y)$.

Electrons are confined within the structure by a suitable potential

The “transverse eigenfunction” (depending on the potential) must obey the boundary conditions

Transverse modes II

Confined electrons (U ≠ 0) in zero magnetic field (B = 0)

nsider first the case of zero magnetic field, so that Eq.(1.6.3) reduces

$$\left[E_s + \frac{\hbar^2 k^2}{2m} + \frac{p_y^2}{2m} + \frac{1}{2}m\omega_0^2 y^2\right]\chi(y) = E\chi(y) \qquad (1.6.4)$$

he eigenfunctions of Eq.(1.6.4) are well-known (see any quantum echanics text such as L. I. Schiff (1968), *Quantum Mechanics*, Third dition, (New York, McGraw–Hill) Section 13). The eigenenergies and genfunctions are given by

$$\chi_{n,k}(y) = u_n(q) \quad \text{where} \quad q = \sqrt{m\omega_0/\hbar}\, y \qquad (1.6.5a)$$

$$E(n,k) = E_s + \frac{\hbar^2 k^2}{2m} + \left(n + \tfrac{1}{2}\right)\hbar\omega_0, \quad n = 0,1,2,\ldots \qquad (1.6.5b)$$

Subbands (as in the MQW)

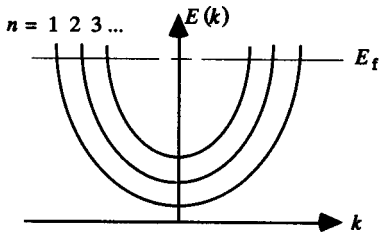

Fig. 1.6.2. Dispersion relation, $E(k)$ vs. k. for electric subbands arising from electrostatic confinement in zero magnetic field. Different subbands are indexed by n.

where $u_n(q) = \exp\left[-q^2/2\right]H_n(q)$

$H_n(q)$ being the nth Hermite polynomial. The first three of these polynomials are

$$H_0(q) = \frac{1}{\pi^{1/4}}, \quad H_1(q) = \frac{\sqrt{2}q}{\pi^{1/4}} \quad \text{and} \quad H_2(q) = \frac{2q^2 - 1}{\sqrt{2}\pi^{1/4}}$$

The velocity is obtained from the slope of the dispersion curve:

$$v(n,k) = \frac{1}{\hbar}\frac{\partial E(n,k)}{\partial k} = \frac{\hbar k}{m} \qquad (1.6.5c)$$

The dispersion relation is sketched in Fig. 1.6.2. States with different index n are said to belong to different subbands just like the subbands that arise from the confinement in the z-direction (see Section 1.2). The spacing between two subbands is equal to $\hbar\omega_0$. The tighter the confinement, the larger ω_0 is, and the further apart the subbands are. Usually the confinement in the z-direction is very tight (~ 5–10 nm) so that the corresponding subband spacing is large (~ 100 meV) and only one or two subbands are customarily occupied. Indeed, in all our discussions we will assume that only one z-subband is occupied. But the y-confinement is relatively weak and the corresponding subband spacing is often quite small so that a number of these are occupied under normal operating conditions. The subbands are often referred to as *transverse modes* in analogy with the modes of an electromagnetic waveguide.

After S.Datta, Electronic Transport in Mesoscopic Systems, Cmbridge (1997)

Quantization (subbands) arises when solving the Schroedinger equation in the confining potential (transverse modes)

Transverse modes III

Calculating the current

To calculate the current we note that the states in the narrow conductor belong to different transverse modes or subbands as discussed in Section 1.6. Each mode has a dispersion relation $E(N,k)$ as sketched in Fig. 2.1.1b with a cut-off energy

$$\varepsilon_N = E(N, k = 0)$$

below which it cannot propagate. The number of transverse modes at an energy E is obtained by counting the number of modes having cut-off energies smaller than E:

$$M(E) = \sum_N \vartheta(E - \varepsilon_N) \qquad (2.1.1)$$

We can evaluate the current carried by each transverse mode (numbered by 'N' in Fig. 2.1.1b) separately and add them up.

Consider a single transverse mode whose $+k$ states are occupied according to some function $f^+(E)$. A uniform electron gas with n electrons per unit length moving with a velocity v carries a current equal to env. Since the electron density associated with a single k-state in a conductor of length L is $(1/L)$ we can write the current I^+ carried by the $+k$ states as

$$I^+ = \frac{e}{L}\sum_k v f^+(E) = \frac{e}{L}\sum_k \frac{1}{\hbar}\frac{\partial E}{\partial k} f^+(E)$$

Assuming periodic boundary conditions (see Fig. 1.2.1 and related discussion) and converting the sum over k into an integral according to the usual prescription

$$\sum_k \rightarrow 2\,(\text{for spin}) \times \frac{L}{2\pi}\int \mathrm{d}k$$

we obtain

$$I^+ = \frac{2e}{h}\int_\varepsilon^\infty f^+(E)\,\mathrm{d}E$$

where ε is the cut-off energy of the waveguide mode. We could extend this result to multi-moded waveguides and write the current, I^+, carried by the $+k$ states in a conductor as

$$I^+ = \frac{2e}{h}\int_{-\infty}^{+\infty} f^+(E)M(E)\,\mathrm{d}E \qquad (2.1.2)$$

where the function $M(E)$ (defined in Eq.(2.1.1)) tells us the number of modes that are above cut-off at energy E. Note that this is a general result independent of the actual dispersion relation $E(k)$ of the waveguide: the current carried per mode per unit energy by an occupied state is equal to $2|e|/h$ (which is about 80 nA/meV).

Contact resistance

Assuming that the number of modes M is constant over the energy range $\mu_1 > E > \mu_2$, we can write

$$I = \frac{2e^2}{h} M \frac{(\mu_1 - \mu_2)}{e} \Rightarrow G_C = \frac{2e^2}{h} M \qquad (2.1.3)$$

so that the contact resistance (which is the resistance of a ballistic waveguide) is given by

$$G_C^{-1} = \frac{(\mu_1 - \mu_2)/e}{I} = \frac{h}{2e^2 M} \sim \frac{12.9\,\mathrm{k\Omega}}{M}$$

Note that the contact resistance goes down inversely with the number of modes. The contact resistance of a single-moded conductor is ~ 12.9 kΩ, which is certainly not negligible! This is the resistance one would measure if a single-moded ballistic conductor were sandwiched between two conductive contacts.

Usually we are concerned with wide conductors having thousands of modes so that the contact resistance is very small and tends to go unnoticed. To calculate the number of modes $M(E)$ we need to know the cut-off energies for the different modes ε_N. As we have seen in Section 1.6, the details depend on the confining potential $U(y)$ and the magnetic field. However, for wide conductors in zero magnetic field the precise nature of the confining potential is not important. We can estimate the number of modes simply by assuming periodic boundary conditions. The allowed values of k_y are then spaced by $2\pi/W$ (see Fig. 1.2.1), with each value of k_y corresponding to a distinct transverse mode. At an energy E_f ($= \hbar^2 k_f^2/2m$), a mode can propagate only if $-k_f < k_y < k_f$. Hence the number of propagating modes can be written as

$$M = \mathrm{Int}\left[\frac{k_f W}{\pi}\right] = \mathrm{Int}\left[\frac{W}{\lambda_f/2}\right]$$

where Int(x) represents the integer that is just smaller than x. Assuming a Fermi wavelength of 30 nm, the number of modes in a 15 μm wide field-effect transistor is approximately 1000, so that the contact resistance is about 12.5 Ω.

The waveguide supports trasnverse modes below some (energy) cut-off, leading to Landauer levels

Electron waveguides

Da G. Timp, Nanotechnology (Springer-Verlag, 1999)

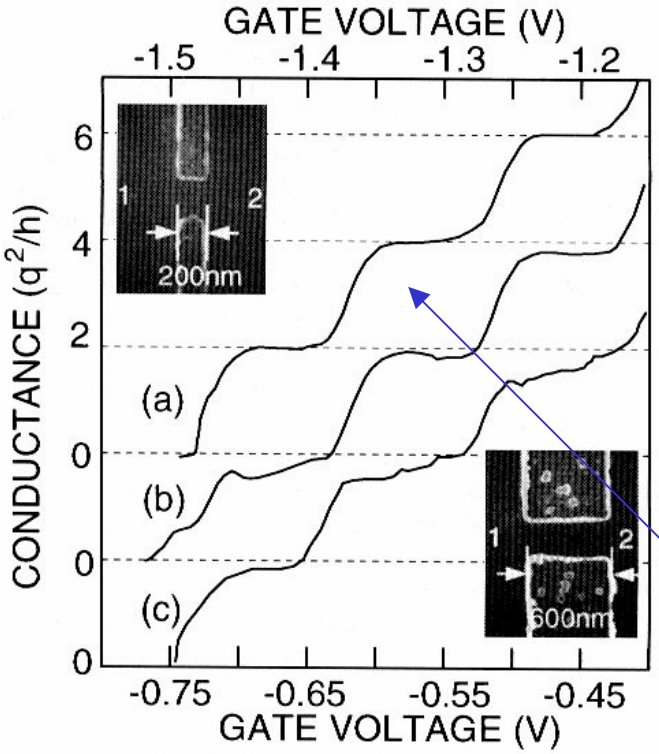

FIGURE 19. The two terminal conductance of an electron waveguide at T=280mK as a function of gate voltage (or the width of the constriction). The inset at the top of the figure shows a top view of 200 nm long split-gate electrodes with a 300 nm gap between them placed on a high mobility *GaAs/AlGaAs* heterostructure. The bottom inset shows a similar device on the same heterostructure with a 600 nm lithographic length. The quantization of the conductance ($\delta G = (1 \pm 0.01) 2q^2/h$) of the 200 nm long constriction shown in (a) deteriorates after cycling to room temperature, as shown in (b). We attribute the deterioration to a difference in the configuration of depletion charges corresponding variations in the width of the constriction. The poor quantization of the conductance of a 600 nm long constriction, shown in (c), is also supposed to develop from fluctuations in the width. (See color plate.)

LANDAUER LEVELS

Da R. Waser Ed., Nanoelectronics and information technology (Wiley-VCH, 2003)

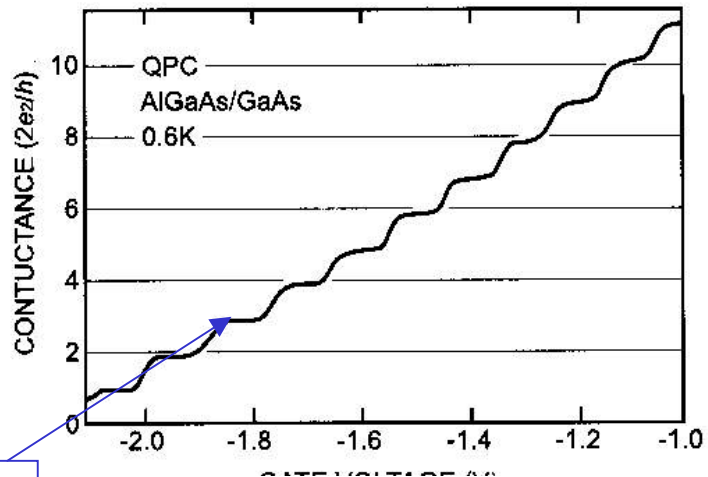

Figure 18: Quantized conductance of a quantum point contact (QPC) at 0.6K prepared at a AlGaAs/GaAs interface (2-DEG). The conductance was obtained from the measured resistance after subtraction of a constant series resistance of 400 Ω (After [8]).

Quantized resistance observed (at very low T)

Relevance of electron waveguides

If conductance is not affected by diffusive transport:
- resistance (within the wire) is negligible;
- speed is at a maximum;
- dissipation can be neglected;
- *single electron transport* can be achieved (no doubt a *single* charge entering the structure is transmitted!)

Quantum wire suitable as unconventional interconnects
(but cumbersome fabrication, need to operate at very low T)

Can the 1DEG transport properties be exploited in a three-terminal (active) device?

Can a 1DEG-channel MOSFET (not just a split-gate) be realized?

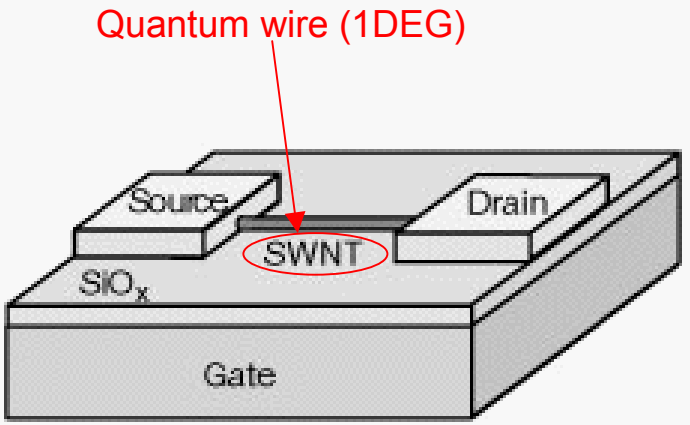

A few words on (single walls) carbon nanotubes (SWCNT)

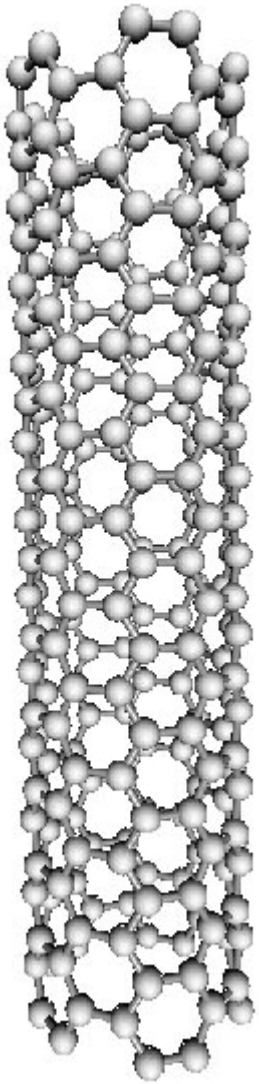

A graphite plane (graphene) is wounded in a cylindrical shape

Preparation methods exist (mostly chemical-physical, e.g., plasma-enhanced CVD or PLD) leading to reasonable fabrication rates and control of the produced structures

Carbon nanotubes exhibit remarkable features for a variety of applications, including mechanical (nanocomposites) and structural (tribology/elasticity)

Carbon nanotubes may exhibit also electronic (conductive/semiconductive) properties of great interest

CNT structure

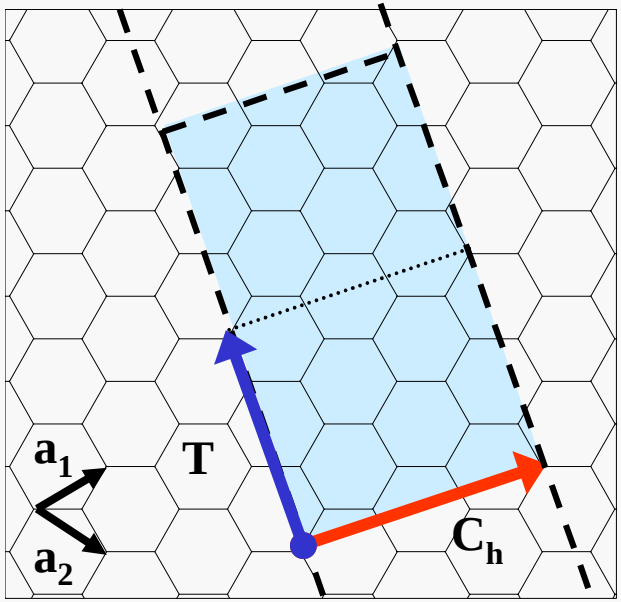

Unit cell described by:

- chiral vector

  $\mathbf{C_h} = n\mathbf{a_1} + m\mathbf{a_2} \equiv (n, m)\ \forall\ n,m \in Z$

- translation vector

  $\mathbf{T} = t_1\mathbf{a_1} + t_2\mathbf{a_2}\ \ \forall\ t_1, t_2 \in Z$

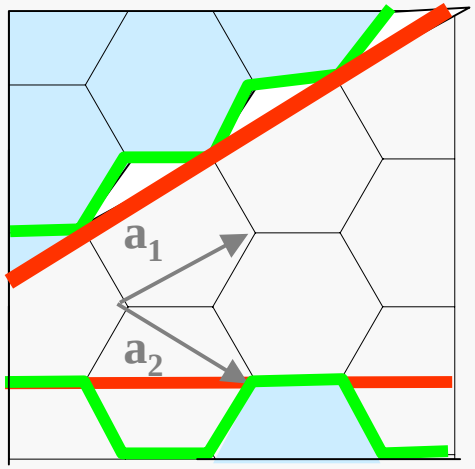

Zigzag (n, 0) tube
$\mathbf{C_h}$ // $\mathbf{a_1}$ (or $\mathbf{a_2}$)

Armchair (n, n) tube

[Chiral (n, m) tube]

CNT diameter: $d_{NT} \propto \sqrt{(m^2 + n^2 + nm)}$

CNT structure uniquely determined by (n, m)

First neighbour distance ~ 1.42 Å

Conductivity in carbon-based materials

See M. McGehee,
www2.latech.edu (Louisiana Tech, 2002))

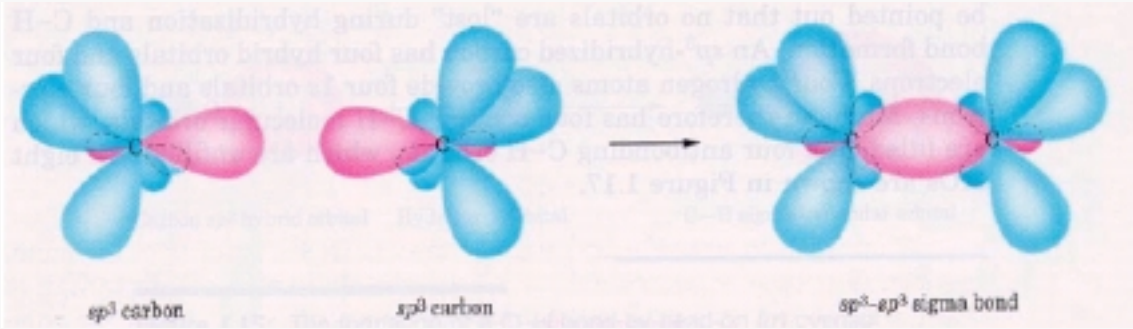

σ bonds between sp^3

Electrons are localized

The behavior is **dielectric**

But…

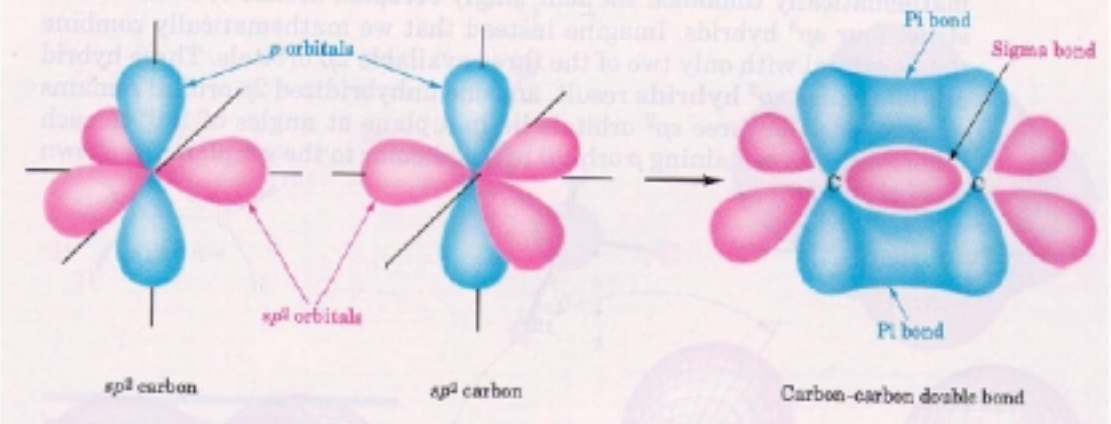

π bonds between sp^2

Electrons get delocalized

The behavior can be **semiconductive**

Electron delocalization may lead to electron transport (*intramolecular*!!)

From graphite to CNT I

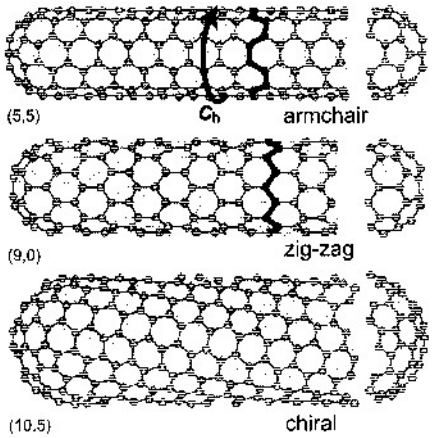

Figure 4: Examples of CNTs with different circumference vectors C_h [5].

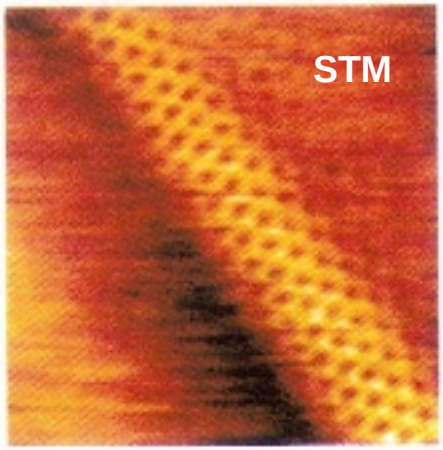

Figure 5: STM image at 77 K of a SWNT at the surface of a rope [6].

Da R. Waser Ed., Nanoelectronics and information technology (Wiley-VCH, 2003)

2.1 Geometrical Structure

The structure of CNTs is described by the circumference vector or **chiral vector C_h**, which represents the full circumference of the tube. It is defined by

$$C_h = n a_1 + m a_2 \quad (1)$$

where a_1 and a_2 are the unit vectors in the hexagonal lattice, and n and m are integers (Figure 1). C_h also defines the propagation vector P_h representing the periodicity of the tube parallel to the tube axis. Furthermore, it settles the so-called chiral angle which is the angle between C_h and a_1. If either n or m are zero, the chiral angle is 0° and the structure is called *zig-zag*. If $n = m$, the chiral angle is 30° and the structure is called *armchair* (Figure 4). All other nanotubes show chiral angles between 0° and 30°. They are known as *chiral* nanotubes because they produce a mirror image of their structure upon an exchange of n and m.

Experimentally, the diameter of nanotubes is frequently determined by TEM, STM or AFM. The chiral structure can be determined by STM (Figure 5).

2.2 Electronic Structure of Graphene

For the discussion of the electronic structure of CNTs, we start again with graphene. As an extension of the description of fused benzene (Chap. 5), in graphene, a bonding π-band and an anti-bonding π*-band is formed from the overlap between $2p_z$-AOs of adjacent atoms. P. R. Wallace [7] derived an expression for the 2-D energy states, W_{2D}, of the π-electrons in the graphene plane as a function of the wave vectors k_x and k_y (see also [8]):

DOS

$$W_{2D}(k_x,k_y) = \pm\gamma_0\left[1+4\cos\left(\frac{\sqrt{3}k_x a}{2}\right)\cos\left(\frac{k_y a}{2}\right)+4\cos^2\left(\frac{k_y a}{2}\right)\right]^{1/2} \quad (2)$$

where γ_0 denotes the nearest-neighbour overlap (or: transfer) integral and $a = 0.246$ nm is the in-plane lattice constant. The two different signs in Eq. (2) represent the π- and π*-band. The calculations show that the π- and π*-band just touch each other at the corners of the 2-D Brillouin zone (Figure 6). In the vicinity of the Γ point, the dispersion relation is parabolically shaped, while towards the corners (K points) it shows a linear $W(k)$ dependence. At $T = 0$ K, the π-band is completely filled with electrons and the π*-band is empty. Because the bands only touch at the K points, integration over the Fermi surface (which is a line for a two-dimensional system) results in a vanishing density of states. On the other hand no energy gap exists in the graphene dispersion relation. This means we are dealing with the unusual situation of a gapless semiconductor. (The real graphite yet is a metal since the bands overlap by approx. 40 meV due to the interaction of the graphene planes.)

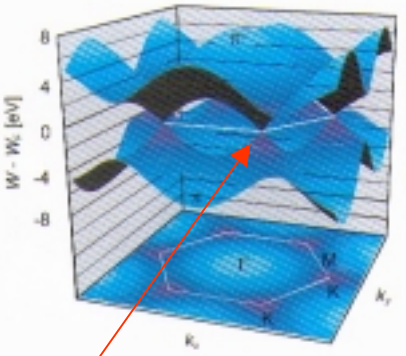

Figure 6: 3-D illustration of the dispersion relation of graphene.

Graphene: zero-gap semiconductor

From graphite to CNT II

DOS and geometry CNT

2.3 Electronic Structure of Carbon Nanotubes

For the description of the band structure of graphene, it has been assumed that the graphene plane is infinite in two dimensions. For CNTs, we have a structure which is macroscopic along the tube axis, but the circumference is in atomic dimensions. Hence, with the density of allowed quantum mechanical states in axial direction will be high, the number of states in the circumferential direction will be very limited. More precisely, the roll-up by the chiral vector $\boldsymbol{C}_h$ leads to periodic boundary conditions in the circumferential direction. Quantum mechanically, these boundary conditions define allowed modes (1-D states) along the tube axis according to:

$$\boldsymbol{C}_h \cdot \boldsymbol{k} = 2\pi j \quad \text{with} \quad |j| = 0, 1, 2, \ldots \tag{3}$$

In the case of arm-chair tubes, the periodic boundary condition yield allowed values for the wave vector in circumferential direction according to:

$$k_{y,j} = \frac{j}{q_y}\frac{2\pi}{\sqrt{3}a}$$

where $q_y = n = m$. For the armchair geometry, the tube axis is identical to the x-direction and the circumference represents the y-direction. As an example of an armchair tube, Figure 7 shows the dispersion relation, the projection of the allowed 1-D states onto the first Brillouin zone of graphene, as well as the $W(k_x)$ relation for a (3,3) tube. Due to the periodic boundary conditions, i. e. by inserting Eq. (4) into Eq. (2), the allowed states condense into lines (black lines in Figure 7a). Here, there are $q_y = 3$ lines on either side of the center of the Brillouin zone and an additional line going through the center. In case of a (3,3) tube the allowed states include the K points. Since the system is now one-dimensional in an electronic sense, different from the case of graphene, the integration over the Fermi surface (which is the sum over the Fermi points) yields a finite density of states at the Fermi energy. The (3,3) tube, and armchair tubes in general, show a *metallic* behavior.

Armchair CNT

As an example of a chiral tube, Figure 8 shows the dispersion relation, the projection of the allowed 1-D states onto the first Brillouin zone of graphene, as well as the $W(k_x)$ relation for a (4,2) tube. We will illustrate why the electronic properties of this (4,2) tube is very different from the (3,3) tube despite their very similar diameters. Again, due to the periodic boundary conditions, the allowed states condense into lines (black lines in Figure 8a). In contrast to the (3,3) tube, the $\boldsymbol{C}_h$ vector is not parallel to the y-direction and, hence, leads to a mixed quantization of k_x and k_y. The propagation of an electron along the tube axis is described by a combination of of k_x- and k_y-components. For this reason, the general letter k is used in Figure 8c, representing the momentum of the electron in the direction of propagation. The band structure of (4,2) tubes is determined by the fact that there are no modes which include the K points of the Brillouin zone of graphene (Figure 8b). The Fermi level is not dependent on the $\boldsymbol{C}_h$ vector, W_F is now in a bandgap, i. e. this type of tube is a *semiconductor*. The bandgap is of the order of a few eV (Figure 8c). In general, the bandgap decreases with increasing diameter of the tube.

Chiral CNT

In general, the semiconducting or metallic behavior of CNTs is controlled by the $\boldsymbol{C}_h$ vector and, hence, by the relation of n and m. Metallic behavior occurs for

$$n - m = 3q \tag{5}$$

Metal/semi

where q is an integer. As a consequence, one-third of all CNTs types are metallic for a statistic distribution of chiralities including all armchair types, since $q = 0$ for them.

The periodic boundary conditions for zig-zag tubes, $(n,0)$ tubes and $(0,m)$ tubes, results in allowed wave vectors according to

$$k_{x,j} = \frac{j}{q_x}\frac{2\pi}{a} \tag{6}$$

The condition for metallic tubes, Eq. (5), is fulfilled for one-third of the tubes, i. e. if n or m are multiples of three. Figure 9 illustrates the density of state (DOS) for two zig-zag type CNTs [9], a (10,0) tube showing a bandgap and, hence, semiconducting behavior (Figure 9a), and a (9,0) tube showing no bandgap and, hence, metallic behavior (Figure 9b).

The discussion so far has been restricted to isolated SWNTs. Theoretical and experimental studies have shown that the intertube coupling within MWNTs and ropes of SWNTs [10], [11] have a relatively small effect on the band structure of a tube [12]. As a consequence, semiconducting and metallic tubes retain their character if they are a part of MWNTs or ropes. By statistical probability, most of the MWNTs and ropes show an overall metallic behavior, because one single metallic tube is sufficient to short-circuit all semiconducting tubes.

SWNT/MWNT

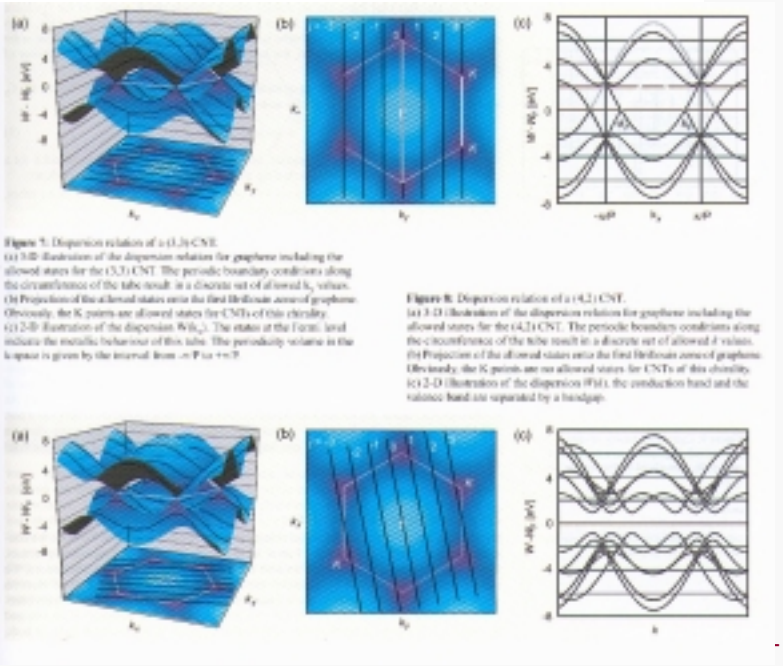

Transport properties depending on the structure:

- armchair (n, n) are conductive
- n – m = 3i (i integer) are semi-metal
- otherwise, semiconductor

EW made of SWCNT

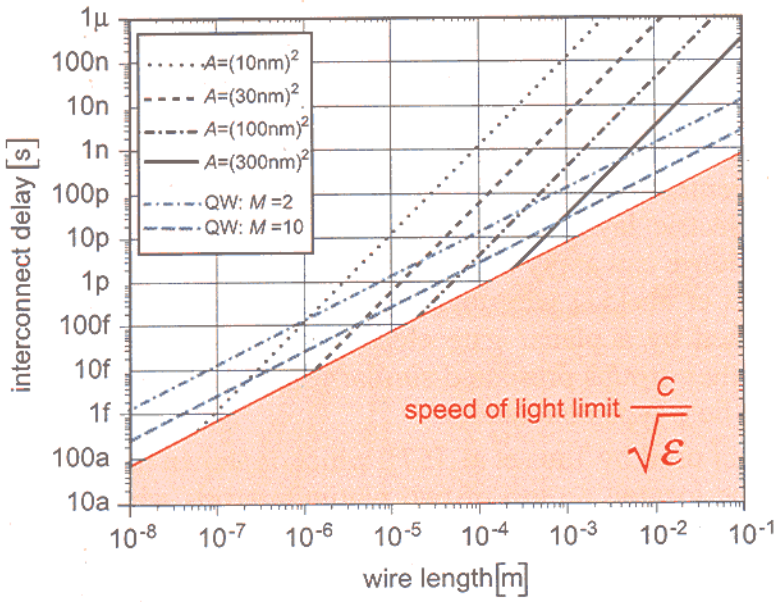

Figure 21: Signal delay in ohmic and ballistic wires as a function of wire length. The black lines represent the delays of ohmic wires with different cross sections A. Surface scattering has been taken into account. For wire lengths smaller than the intersections of black and red lines, the delay is governed by the speed of light and the relative permitivity of the dielectric. The nanotube wires display a completely different behavior to the ohmic wires, as shown by the blue lines. Due to the length-independent resistance, nanotubes exhibit better delay values for longer wires. *M* represents the number of conductive channels, that can be formed either by the number of occupied energy levels or by the number of shells of a multi-wall nanotube.

480

Thanks to the intramolecular conductivity, CNT wires are suited also for long travel transport (speed, dissipation,…)

Active devices with quantum wires (CNT) I

5.1 Comparison to MOSFETs

The success of modern silicon technology is owed, to a large extent, to MOSFETs and the CMOS concept in which circuits draw current only during the switching action and are thus the indispensable ingredients for low power complex circuits like processors and controllers. The inversion channel of MOSFETs can be considered as a 2-D conduction system. Electron motion in the inversion channel is not *apriori* restricted in planes but due to high gate fields the motion perpendicular to the gate plane is quantized giving rise to subband formation. The conductive channel can be considered as a 2-D electron gas. At room temperature many subband levels contribute to the current transport enabling a high driving capability and switching speed.

Semiconducting carbon nanotubes can be operated in a gate electrode configuration in a similar way to silicon MOSFETs. The electronic properties of CNTs have been described in Sec. 2. The excess electrons are delocalized and form a highly conductive π-electron system. Unlike in silicon MOSFETs the electron system of a nanotube is 1-D. Placing a field electrode next to the nanotube one can influence its conductivity by the accumulation or depletion of electrons provided that the electron density is not to high (the tube is semiconducting). This configuration is called CNTFET, in analogy to the silicon field effect transistor. As the electrical characteristics of carbon nanotubes strongly depend on their chirality, diameter and doping, the characteristics of CNTFETs can be controlled by choosing the appropriate morphology of the CNT. Single-wall semiconducting tubes are best suited for CNTFETs because their electron system is not bypassed by inner shells.

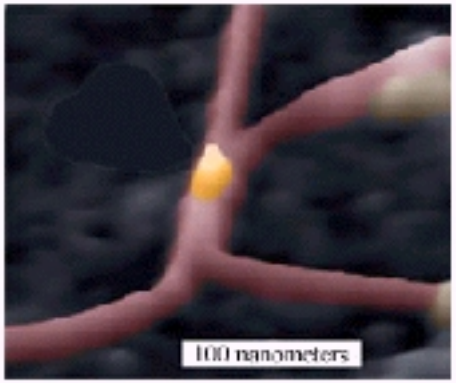

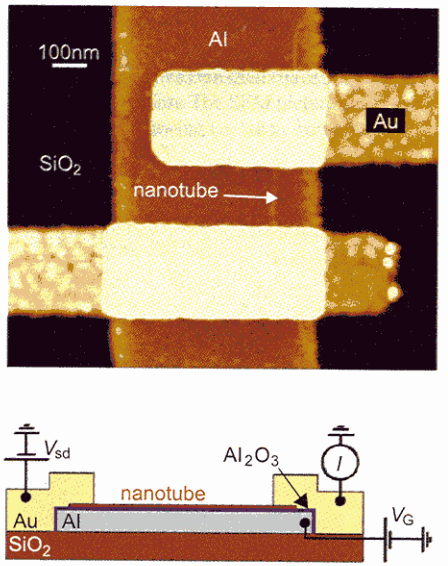

Figure 28: Isolated back-gate CNTFET. The gate is realized by an Al-strip on top of SiO_2. The gate oxide is the naturally grown thin Al_2O_3 layer on top of the Al-strip. Source and drain contacts are made by Au deposition ([64]).

Active devices with quantum wires (CNT) II

Figure 25: A carbon nanotube field effect transistor (CNTFET). The nanotube (red) is located on top of two platinum contacts (yellow). The back-gate-stack (blue) is formed by a silicon dioxide dielectric on top of a silicon wafer (colored AFM-image taken from [57]).

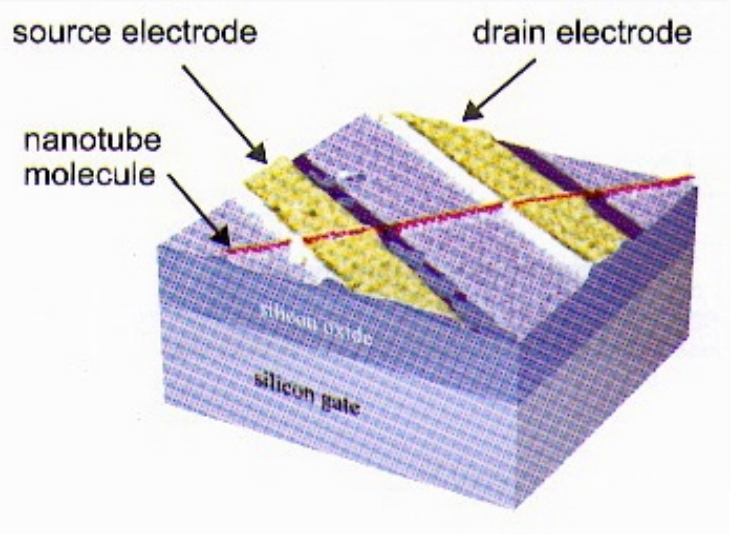

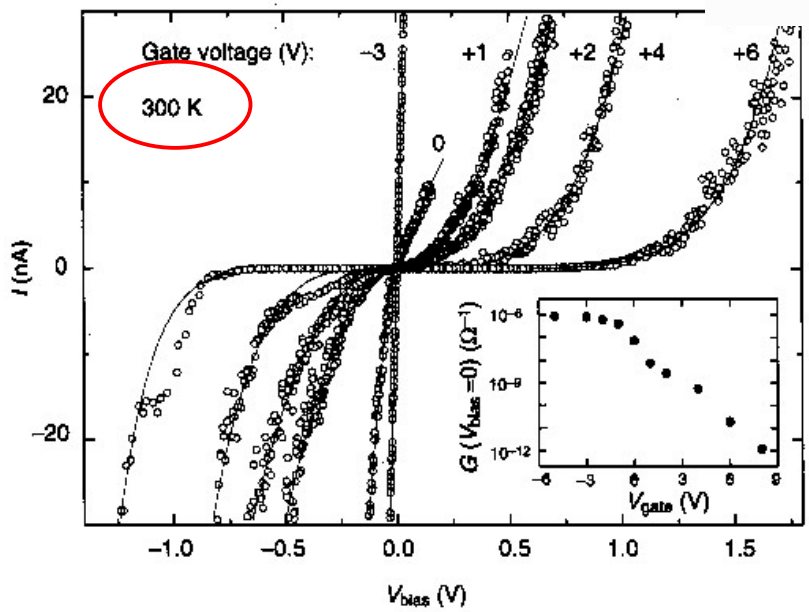

Figure 26: The current-voltage characteristics of a semiconducting single-wall carbon nanotube for different gate voltages (see Figure 25). For large positive gate voltages the conductance of the tube is very small for source-drain biases less than approximately 1 V. Changing the gate voltage to negative values increases the conductivity steadily until saturation is reached at approximately –3 V (see insert). The maximum conductivity is comparable to the values found for metallic tubes measured in the same experiment (taken from [57]).

Room temperature operation

Conclusions

✓ Transport properties (conductivity) is strongly affected by dimensionality

✓ Lower dimensionality implies a different functional dependence of DOS on the energy

✓ Quantum confinement effects may arise when considering nanostructures with size comparable to the de Broglie wavelength (either single-particle, or degenerate semiconductors)

✓ Quantum Hall Effect (2DEG + magnetic field) demonstrates quantized resistance

✓ Similar quantization effects (but for factor 2!) is observed also in electron waveguides

✓ Landauer levels can be associated to transverse modes

✓ Carbon nanotubes may be a good route to achieve “molecular” quantum wires (exploitable in both interconnects and CNTFET)